
Article:
Goulas, A. orcid.org/0000-0002-4203-8547, Whittaker, T. orcid.org/0000-0001-8099-273X, Chi-Tangyie, G. et al. (4 more authors) (2023) Multi-material additive manufacture and microwave-assisted sintering of a metal/ceramic metamaterial antenna structure. Applied Materials Today, 33. 101878. ISSN 2352-9407

https://doi.org/10.1016/j.apmt.2023.101878

Applied Materials Today 33 (2023) 101878

Contents lists available at ScienceDirect

Applied Materials Today

journal homepage: www.elsevier.com/locate/apmt

Multi-material additive manufacture and microwave-assisted sintering of a metal/ceramic metamaterial antenna structure

Athanasios Goulas [a,*], Tom Whittaker [b], George Chi-Tangyie [a], Ian M. Reaney [c], Daniel Engstrøm [b], Will Whittow [b], Bala Vaidhyanathan [a]

[a] Department of Materials, Loughborough University, Loughborough LE11 3TU, United Kingdom
[b] Wolfson School of Mechanical, Electrical and Manufacturing Engineering, Loughborough University LE11 3TU, United Kingdom
[c] Department of Materials Science and Engineering, University of Sheffield, Sheffield S1 3JD, United Kingdom

ARTICLE INFO

Keywords:
Multi material additive manufacturing
Metal/ceramic structures
Microwave sintering
Metamaterials

ABSTRACT

Multi-material metal/ceramic 3D structures comprising of metallic silver and ultra-low sintering temperature silver molybdenum oxide ceramics, have been additively manufactured and hybrid densified using microwave-assisted sintering for the first time. Optimum densification conditions at 440 °C / 1 h, resulted in relative permittivity, $\varepsilon_r = 10.99 \pm 0.04$, dielectric losses, $\tan\delta = 0.005 \pm 0.001$ and microwave quality factor, $Q \times f = 2597 \pm 540$ GHz. Applying 2 kW microwave energy at 2.45 GHz for 60 min, was proven sufficient, to densify the metallic Ag infilling electrodes, without causing any macroscopic defects. A fully functional multi-layered antenna structure with a metamaterial artificial magnetic conductor was designed, dual-printed and densified, to showcase the potential of combining multi-material additive manufacturing with microwave-assisted sintering.

1. Introduction

Microwave (MW) dielectric ceramics, have for a long time been established as the go-to materials, for applications related to mobile and wireless telecommunications, such as dielectric substrates, dielectric resonators, filters, capacitors, global positioning, and Wi-Fi components [1–3].

Their properties namely: relative permittivity (ε_r, whose optimum value is specific to the application), low dielectric loss tangent ($tan\delta$) and high-quality factor ($Q \times f$) are of particular interest to modern applications in 5 G and 6 G telecommunication systems.

Most MW ceramics require sintering temperatures above 1000 °C, making them incompatible with low-cost electrode materials such as Ag and Al. Low sintering and ultra-low sintering temperature co-fired ceramics (LTCCs/ULTCCs) are envisaged to revolutionise how modern ceramic components and devices are manufactured, where the temperature requirements for their densification could be as low as 400–500 °C, thus making it possible to co-fire both electrode and dielectric materials together.

The oxide compounds in the Ag_2O – MoO_3 system, have been highlighted before as excellent candidates for manufacturing ULTCC systems and devices. Zhou et al. were the first to investigate the binary system which contains $Ag_2Mo_4O_{13}$, $Ag_2Mo_2O_7$ and Ag_2MoO_4 phases. The latter (Ag_2MoO_4) was reported to sinter at 450 °C, resulting in $\varepsilon_r = 8.08$ and $Q \times f = 17{,}000$ GHz [4].

Additive manufacturing (AM), commonly known as 3D printing, has shown great promise and the potential to revolutionise how modern electronics are manufactured. Certain AM technologies such as multi-material extrusion[5,6], can deposit more than one dissimilar material (i.e. metals and ceramics) in a single manufacturing process, enabling the production of an entire functional component in single processing step, achieving structures not possible through conventional methods. This is often followed by a post-processing step, using conventional sintering at a low temperature. However additively manufactured components do not always achieve bulk material properties, due to processing limitations and in the case of metal/ceramic components, they also suffer from distortion and warpage due to the mismatch of coefficient of thermal expansion (CTE) during the conventional sintering.

Microwave assisted sintering (MAS), has gained great attention given its capability to rapidly heat and densify various materials [7–10]. This offers great advantages in terms of speed, energy efficiency, process simplicity and significantly lowers the environmental impact and carbon footprint of the post-processing stage [11].

* Corresponding author.
E-mail address: a.goulas@lboro.ac.uk (A. Goulas).

https://doi.org/10.1016/j.apmt.2023.101878
Received 15 May 2023; Received in revised form 16 June 2023; Accepted 1 July 2023
Available online 5 July 2023

This study investigates the microwave dielectric properties of Ag_2MoO_4 fabricated through material extrusion, an additive manufacturing process, together with the use of microwave assisted sintering of metal/ceramic structures, prepared via multi-material extrusion additive manufacturing. The effect of a) sintering temperature on the physical and dielectric properties for the ceramic test samples and b) microwave processing on the densification effect of metal/ceramic test structures is discussed.

2. Materials & methods

2.1. Materials

The Ag_2MoO_4 (AMO) powder was synthesised using the solid-state reaction method. High purity raw chemicals, Ag_2O (99.5%, Acros Organics) and MoO_3 (>99%, Acros Organics) were weighed stoichiometrically and then ball-milled in isopropanol for a duration of 4 h. Afterwards, the mixed powders were dried and calcined accordingly. The calcined powder was then ball milled using a rotary mill and sieved through a 100 μm aperture laboratory sieve.

Silver powder (Sigma Aldrich, UK) was used as the electrode material, to 3D print the conductive parts of the demonstrator antenna structure. The powder comprised of Ag nanoparticles, with an approximate particle size of $d_{50} = 5$ μm.

2.2. Synthesis of printable materials

A binder mix consisting of ethylene glycol diacetate (3.3 wt.%, Sigma Aldrich, UK) as non-ionic dispersant, methylcellulose (1.6 wt.%, Sigma Aldrich, UK) and propylene carbonate (0.9 wt.%, Sigma Aldrich) as viscosity modifier and binder, diisononyl phthalate (1.3 wt.%, Sigma Aldrich, UK) as plasticiser, and ammonium lauryl sulphate (< 0.5 wt.%, Sigma Aldrich, UK) as surfactant was prepared. The AMO powder was slowly incorporated into the binder followed by mixing and then topped up with de-ionised water. The paste was homogenised using a planetary mixer (Thinky ARM 250, Thinky Inc., Laguna Hills, California USA) at 2000 rpm for 2 min. The total solids content in the AMO paste was 80 wt.%. The same binder mix and mixing process were used for the synthesis of a silver-based printable electrode material. The total solids content in the Ag paste was 50 wt.%.

2.3. Additive manufacturing and post-processing

All additively manufactured test samples and the demonstrator metamaterial antenna structure, were made using a multi-process additive manufacturing kit (High-Resolution Engine, Hyrel3D, Norcross, GA, USA), equipped with syringe dispensing modules (SDS-5, Hyrel3D, Norcross, GA, USA), using 5 ml luer-lock syringes (Becton Dickinson, Franklin Lakes, New Jersey, USA) and 500 μm metallic needles of 18.25 mm in length (Adhesive Dispensing, Milton Keynes, United Kingdom). A printing speed of 5 mm/s, layer thickness of 0.2 mm, 0.45 mm hatch spacing; providing a 10% overlap of the extruded filaments, and a constant positive displacement value of 85 pulses per microlitre for the AMO paste and 50 pulses per microlitre for the Ag paste, were used to print cylindrical test samples of 10 mm in diameter and 4 mm thickness. The test samples were first modelled prior to printing using CAD and the G-code was produced via Hyrel3D' s inbuilt slicing software (Repetrel, Hyrel3D, Norcross, GA, USA).

3D printed samples were left to dry at room temperature for a minimum of 24 h. Samples were thermally debinded in a furnace (RHF 1600, Carbolite Gero Ltd, Hope, UK) in static air using a ramp rate of 1 °C·min^{-1} up to 400 °C whilst holding at 100, 200, 300 and 400 °C for 2 h each.

The debinded ceramic and metal/ceramic samples were densified in a multimode hybrid furnace by applying microwaves of 2 kW power at 2.45 GHz (CEM Microwave Technology Ltd., Buckingham, UK) in the temperature range of 420–480 °C, under static air. Heating and cooling rates of 3 °C·min^{-1} were used.

2.4. Characterisation methods

The phase assemblage and crystal structure of the as-synthesised powder and sintered AMO ceramics were investigated using X-Ray diffraction (D2 Phaser, Brucker AXS, Karlsruhe, Germany) using CuKα radiation at $\lambda = 1.54054$ Å, operating at 30 kV and 10 mA. A 1 mm divergence, 2.5° Soller and a 3 mm air-scatter slits were used. Diffraction patterns were collected in the 10–60° 2ϑ interval, using a 0.02° step size and 15 min^{-1} sample rotation. Data were analysed using Brucker's proprietary software (DIFFRAC.EVA 6.1, Brucker AXS, Karlsruhe, Germany).

The quantitative weight fraction analysis of the identified phases of the as-synthesised AMO powder, was estimated using a graphical user interface of the BGMN kernel for Rietveld refinement of PXRD data (Profex 5.2.0, Solothurn, Switzerland).

The density of the sintered samples was measured using the Archimedes principle with deionised water as the immersion medium. The samples' mass was measured using a balance fitted with a density measurements kit (ME204, Mettler-Toledo, Leicester, UK). Results are reported as an average of three different 3D printed samples, together with standard deviation (σ).

The effect of processing on surface microstructure of the metal/ceramic structures was assessed using a scanning electron microscope (SEM) (TM3030, Hitachi High Energy Technologies, etc.). To prevent charging during SEM, samples were sputter coated with a gold/palladium alloy in an 80:20 wt.% ratio, for 60 s at 25 mA (Quorum Q150T, Quorum, Edwards, Hastings, UK).

Relative permittivity (ε_r), quality factor ($Q \times f$) and dielectric loss tangent ($tan\delta$) of additively manufactured sintered samples at microwave frequencies were determined by placing the cylindrical 3D printed test samples of 10 mm diameter and 4 mm thickness, into a 24 mm $TE_{01\delta}$ cavity resonator (QWED, Warsaw, Poland), measuring the transmission and reflection from the target sample, connected to a Vector Network Analyser (VNA) (MS465B22, Anritsu, Japan) using coaxial cables [12]. The properties were calculated using QWED's proprietary software. Results are reported as an average of 3 different 3D printed samples, together with standard deviation (σ). To eliminate the influence of porosity on the bulk permittivity of the additively manufactured test samples, the following equation was used [13]:

$$\varepsilon_{corrected} = \varepsilon_{measured} \times 1 + (1.5 \times \text{Porosity}) \quad (1)$$

The reflection coefficient of the demonstrator antenna structure was measured with an Anritsu Vector Network Analyser (VNA) (MS465B22, Anritsu, Japan). The directivity and gain radiation patterns and efficiency were then measured in a near field anechoic chamber (NSI-MI UK, Dronfield, UK).

3. Results and discussion

3.1. Raw material characterisation

Fig. 1 presents the room-temperature diffraction patterns of the AMO powder. The main diffraction peaks were indexed to the cubic (spinel) β-Ag_2MoO_4 phase (ICDD PDF 00–08–0473) with $Fd\bar{3}m$ space group symmetry, lattice parameter $a = 9.3127$ Å and theoretical density 6.178 g·cm^{-3}. Two peaks at 38.11° and 42.77° 2ϑ were indexed to the (1 1 1) and (2 0 0) lattice plains of the cubic Ag phase (ICDD PDF 00–04–0783) with $Fm\bar{3}m$ group, lattice parameters $a = 4.0862$ Å and a theoretical density of 10.5 g·cm^{-3}. The remaining peaks at 28.3° and 29° 2ϑ, were indexed to the (0 2 0) and (−1 −2 2) triclinic (anorthic) $Ag_2Mo_2O_7$ (ICDD 00–075–1505) with $P\bar{1}$ space group, lattice parameters $a = 6.095$ Å, $b = 7.501$ Å, $c = 7.681$ Å, $\alpha = 110.4°$, $\beta = 93.3°$ and $\gamma = 113.5°$ and a

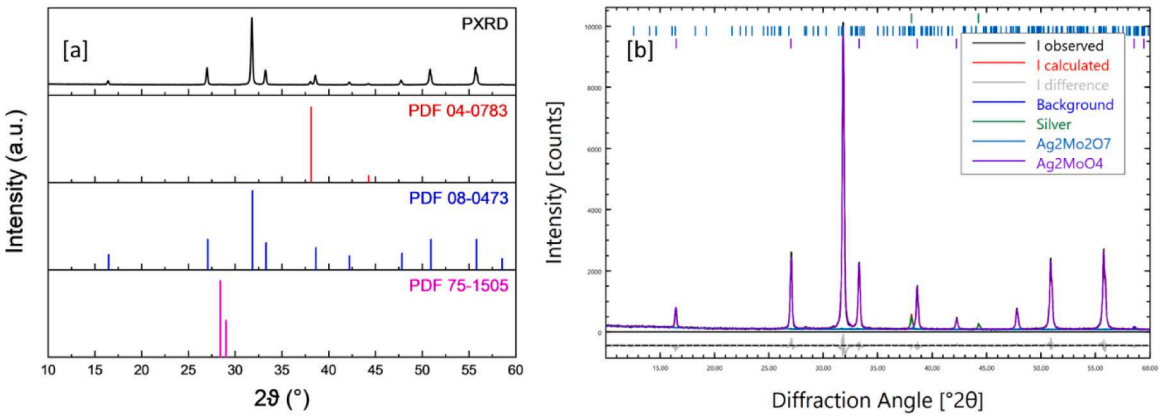

Fig. 1. [a] Room temperature X-ray diffraction patterns and [b] Rietvield refinement of the as-synthesised AMO powder.

theoretical density of 5.9 g·cm^{-1}.

Table 1 contains a quantification estimate (wt.%) of the identified phases in the as-synthesised AMO powder, following the BGMN Rietveld refinement procedure [14]. The crystallography open database entries for β-Ag_2MoO_4 phase (COD 41,247,775), Ag (COD 110,136) and $Ag_2Mo_2O_7$ (COD 4,027,813) were used. The presence of metallic Ag in the AMO mixture is assumed to be due to the decomposition of excess Ag_2O, during the calcination process. Based on the phase quantification, the final density of the AMO powder was calculated at 6.297 g·cm^{-3}.

3.2. Physical and microwave dielectric properties of AMO ceramics

Fig. 2 contains the room-temperature diffraction patterns of the 3D printed and microwave sintered ceramic samples, as a function of their sintering temperature. All peaks were indexed to the previously identified crystalline phases of Ag, Ag_2MoO_4 and $Ag_2Mo_2O_7$. Further quantification of the identified phases was not pursued, due to non-satisfactory fitting of the identified phases.

Fig. 3, presents the effect of sintering temperature, on the density and microwave dielectric properties of the additively manufactured AMO ceramic test samples, at 420–480 °C. Sintering experiments past 480 °C were not pursued, due to the possible deterioration of the AMO's properties, as reported in previous studies [4,6,15]. Both density (ρ) and relative permittivity (ε_r) increase as a function of sintering temperature, with the highest values of $\rho = 5.57 \pm 0.03$ g·cm^{-3} and $\varepsilon_r = 10.99 \pm 0.04$ achieved at the sintering temperature of 480 °C. The reported values are lower, compared to previously published data [6,15], due to the overall low densification; $\rho_{rel} = 88.45 \pm 0.48\%$, that was achieved. It should be noted however, that following a correction for porosity [4] the relative permittivity values, are in good agreement with previously reported data. A combination of potential defects during both the green forming and sintering stages, such as: non-continuous material deposition (commonly known as misextrusion), or a mismatch between the grain growth mechanisms of the apparent AMO phases, may have contributed to the overall low densification.

The quality factor ($Q \times f$) values of AMO ceramic test samples decrease from 2095 ± 520 GHz to 1546 ± 156 GHz, with increasing sintering temperature from 440 °C to 460 °C and then continuously increase up to 2597 ± 540 GHz for the sintering temperature of 480 °C. $Q \times f$ values are affected by a great number of factors such as the porosity, grain boundaries, variance between in the grain size, random crystal orientation, impurities, anharmonic lattice vibrations, various defects such as micro-cracks [16,17]. We note that $Q \times f$ values are notably lower, compared to previously published data. It is hypothesised that in combination with the intrinsic and extrinsic factors mentioned above, the small amounts of metallic silver present within the bulk of AMO; as discussed in Section 3.1, may have contributed towards the overall increase in the material's dielectric losses; since the dispersed silver particles are not only MW absorbing [10,18] but also have a large interfacial contact area with the ceramic matrix. Such interfacial regions are known sources of loss. However, given the overall statistical variance of the measured values, $Q \times f$ values could be considered relatively stable supported by the small deviation in the tanδ values. In summary, additively manufactured AMO samples, sintered at 480 °C for 1 h, exhibited optimal microwave dielectric properties of $\varepsilon_r = 10.99 \pm 0.04$, $Q \times f = 2597 \pm 540$ GHz. Table 2, lists all measured properties of the AMO ceramic samples.

Table 1
Phase quantification (wt.) of the as-synthesised AMO powder and Rietveld refinement fitting parameters.

β-Ag_2MoO_4 (wt.%)	$Ag_2Mo_2O_7$ (wt.%)	Ag (wt.%)	R_{wp}	R_{exp}	χ^2
96.29 ± 0.01	0.89 ± 0.01	2.82 ± 0.01	8.66	7.23	1.43

3.3. Additive manufacture and field-assisted sintering

A series of hybrid microwave and convention sintering experiments were conducted to identify the optimum processing conditions that would allow densification of a printed conductive layer, without unwanted macroscopic defects such as warpage, given the inherent mismatch in the thermal expansion coefficient of the two different materials. This approach was based on the selective microwave absorptive nature, of the two different materials. With silver being a good absorber of microwave energy [18,19], while AMO would appear to be virtually transparent at microwave frequencies, given its ultra-low dielectric loss [20]. The two materials (Ag and AMO) have previously been found to be chemically compatible [4,6]

Following the debinding cycle, a series of metal/ceramic printed structures were slowly ramped up to 480 °C and were then exposed to microwaves for a total duration of 30–90 min. All processed metal/ceramic test samples appeared to be fully sintered, however exposure to microwaves for a time longer than 60 min, led to warpage of the metal/ceramic structures, post sintering. Fig. 4 presents scanning electron micrographs from the surface of the co-sintered metal/ceramic test samples. The silver particles of the electrode counterpart of the metal/ceramic structure were shown to be well bonded together.

3.4. Additive manufacture of a prototype multi-layered metamaterial antenna

To demonstrate the suitability of this material for multi-material direct ink writing, a multi-layered antenna was designed with an artificial magnetic conductor (AMC). The structure consists of a quarter wavelength monopole fed with a co-planar waveguide (CPW) transmission line which is backed with an AMC. AMCs are often deployed to

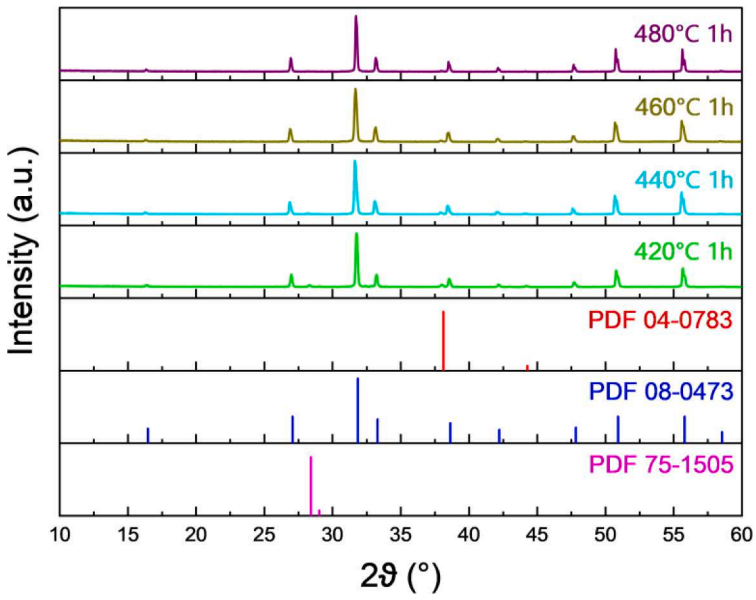

Fig. 2. X-Ray diffraction patterns of the AMO 3D printed samples.

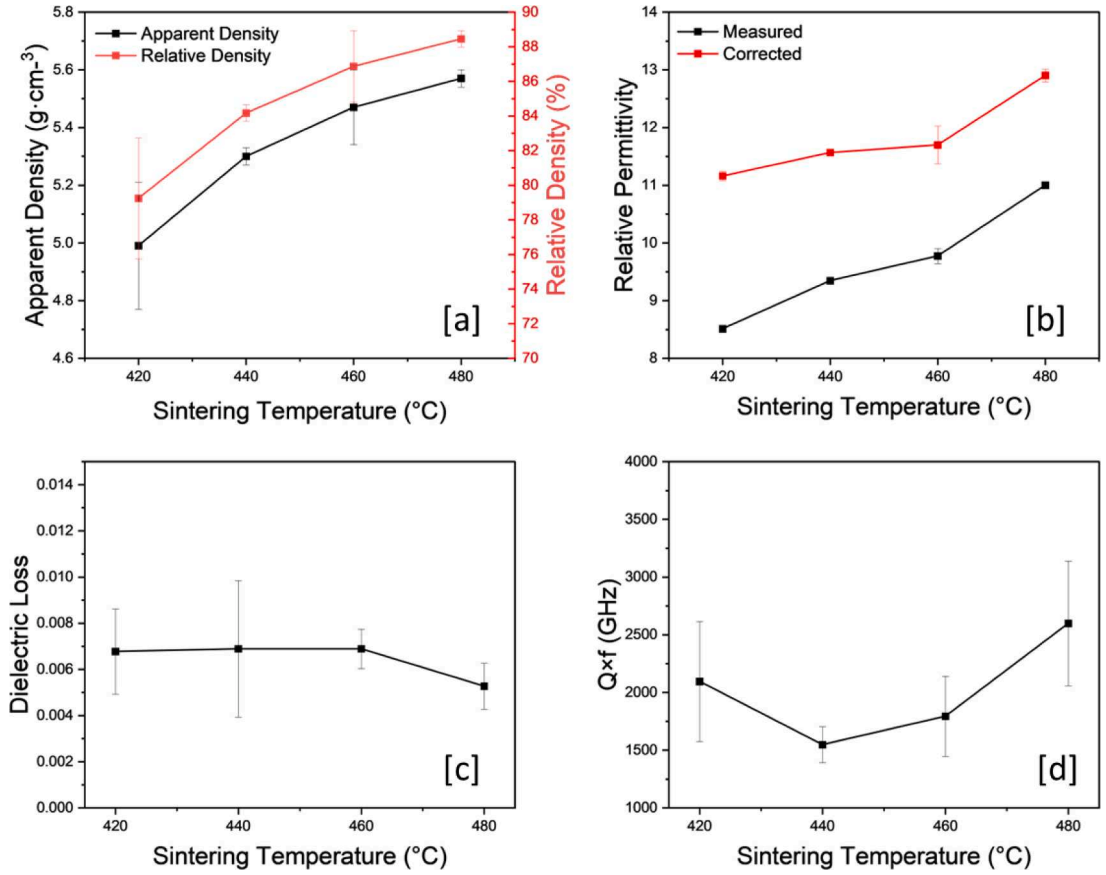

Fig. 3. The effect of sintering temperature on the microwave dielectric properties of additively manufactured AMO ceramic samples: [a] apparent and relative density, [b] relative permittivity (ε_r, $\varepsilon_{corrected}$), [c] dielectric loss tangent (tan δ), and [d] quality factor ($Q \times f$).

increase the directivity and gain of some low gain antennas by ensuring the reflections from the ground plane are in phase with the incident excitation. They can be placed very close to the radiating antenna thus they are often used in low profile applications such as wearable antennas as the AMC is deployed to improve radiation efficiency by redirecting electromagnetic radiation away from the human body.

Monopoles and AMC structures are resonant and thus have reasonably narrow bandwidths; hence it may be a possibility that uneven shrinkage during the sintering process may cause different frequency shifts for the monopole and AMC (since shrinkage will change the resonant frequency of both parts). To reduce complication associated with shrinkage, a wideband monopole design was used; this increases

Table 2
The sintering temperatures, microwave dielectric properties of relative permittivity (εr), dielectric loss tangent (tanδ), quality factor (Q × f) and densities of the additively manufactured and field-assisted sintered AMO ceramic samples.

Temperature (°C)	Frequency (GHz)	Relative Permittivity ± σ	tanδ ± σ	$Q \times f \pm \sigma$ (GHz)	Density ± σ ($g \cdot cm^{-3}$)	Relative Density ± σ (%)	Corrected Relative Permittivity ± σ
420 / 1h	11.50	8.51 ± 0.03	0.006 ± 0.0004	2095 ± 520	4.99 ± 0.22	79.24 ± 3.49	11.16 ± 0.08
440 / 1h	11.47	9.34 ± 0.01	0.006 ± 0.002	1546 ± 156	5.3 ± 0.03	84.17 ± 0.48	11.56 ± 0.04
460 / 1h	11.53	9.77 ± 0.13	0.006 ± 0.0008	1793 ± 347	5.47 ± 0.13	86.87 ± 2.06	11.70 ± 0.33
480 / 1h	11.50	10.99 ± 0.04	0.005 ± 0.001	2597 ± 540	5.57 ± 0.03	88.45 ± 0.48	12.90 ± 0.11

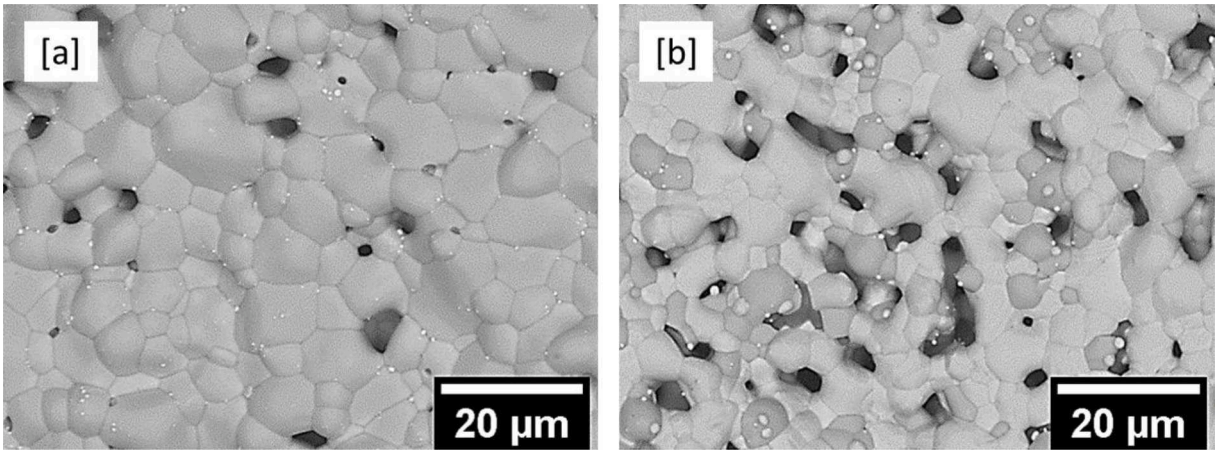

Fig. 4. Scanning electron micrographs from the surface of the [a] AMO ceramic and [b] Ag electrode, hybrid co-sintered at 480 °C / 60 m.

the bandwidth of the monopole and thus make the overall design less susceptible to uneven shrinkage.

The demonstrator consists of five layers, from top to bottom: the antenna, a separation layer of ceramic, a layer of conductive square loops, another ceramic separation layer, and finally a ground plane; the final 3 layers form the AMC structure. The complete demonstrator design can be seen in Fig. 5a.

AMO ceramic was used for the dielectric and a silver-based ink was used for the 3D printed conductor. The green body was printed onto an alumina tile; for this reason, the ground plane was formed from a section of copper tape, since any silver-based electrode ink printed directly on the alumina tile would be irreversibly bonded to the alumina during the sintering process.

The AMC consists of a 5 × 5 array of square loops; each loop is 3.5 mm across, the loop thickness is 0.5 mm, the loop separation is 0.5 mm and the conductor thickness is 0.2 mm; the dimensions are shown in Fig. 5b. The square loop layer is also separated from a copper tape ground plane by a 0.8 mm layer of AMO ceramic. The wideband monopole is fed by a 50 Ohm CPW transmission line which broadens out to the wideband monopole, the dimensions of the monopole are shown in Fig. 5c.

Afterwards an SMA connector was attached, and connections made with a high conductivity, air curing, silver-based ink (Voxel 8, Somerville, Massachusetts, US) which has a datasheet conductivity of 2 MS/m. The dimensions of the antenna were measured after firing and the sample had shrunk by approximately 12.5%; the electromagnetic simulation using CST Microwave Studio software was then conducted with the actual printed dimensions. Fig. 6 shows the printing of the metal/ceramic antenna and Fig. 7 the resultant structure before and after densification.

From the reflection coefficient shown in Fig. 8, the measured demonstrator is not particularly well matched to the 50 Ohm source; the most likely cause from small inaccuracies in the dimensions during the printing process and shrinkage during densification. However, the

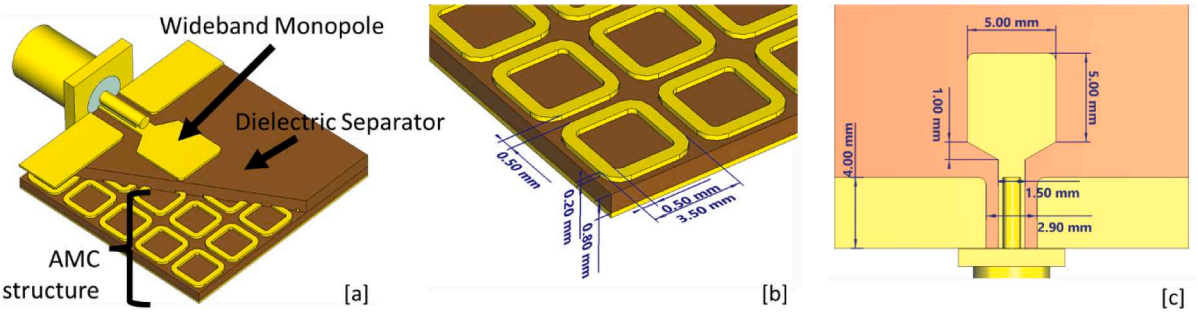

Fig. 5. CAD diagram of the [a] wideband monopole demonstrator with AMC (note the ceramic layer below the monopole has been made partially transparent to show the whole structure). The monopole is fed with an SMA connector which transitions to a coplanar waveguide transmission line. Dimensions of the [b] square loops as part of the AMC, and [c] the wideband monopole antenna layer.

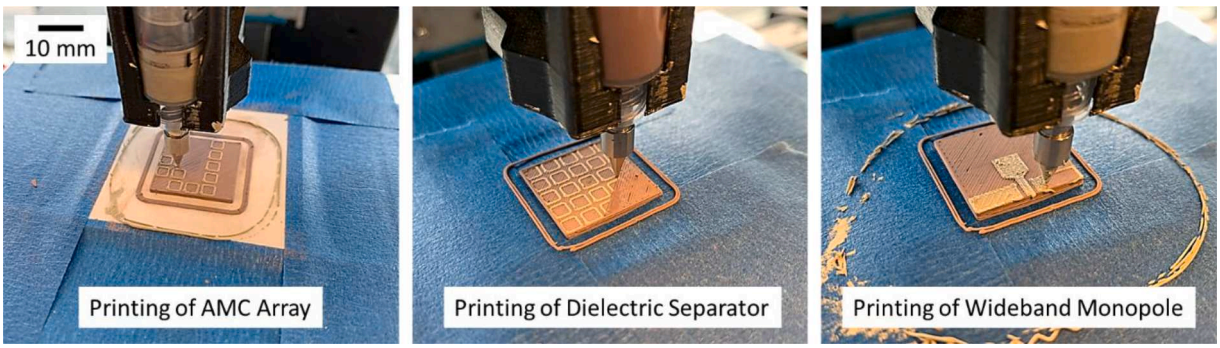

Fig. 6. Photos from the printing the different layers of the AMC antenna structure.

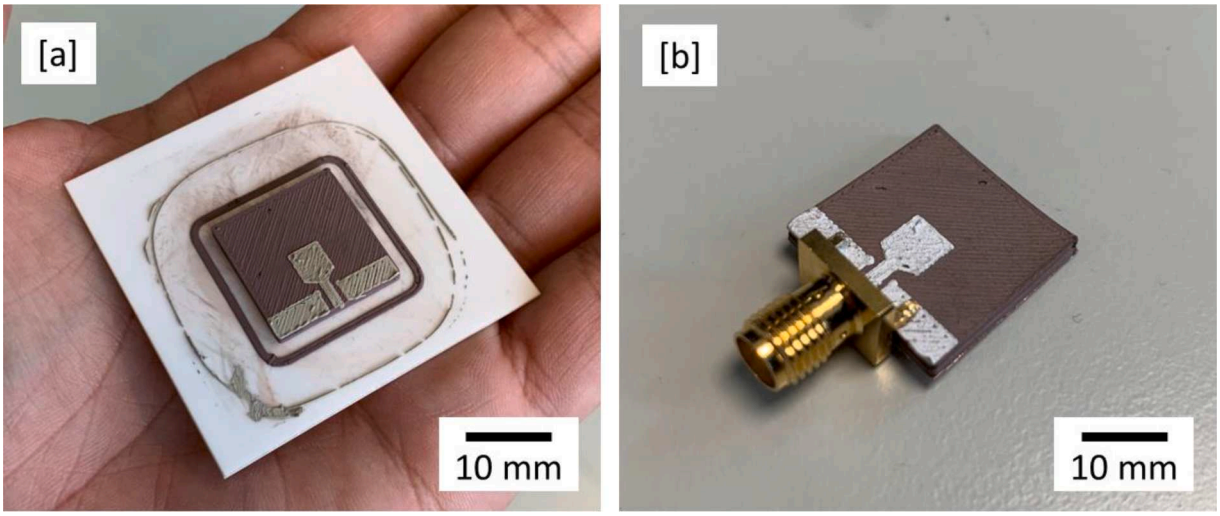

Fig. 7. 3D printed AMC antenna structure in [a] green and [b] sintered state with an attached SMA connector.

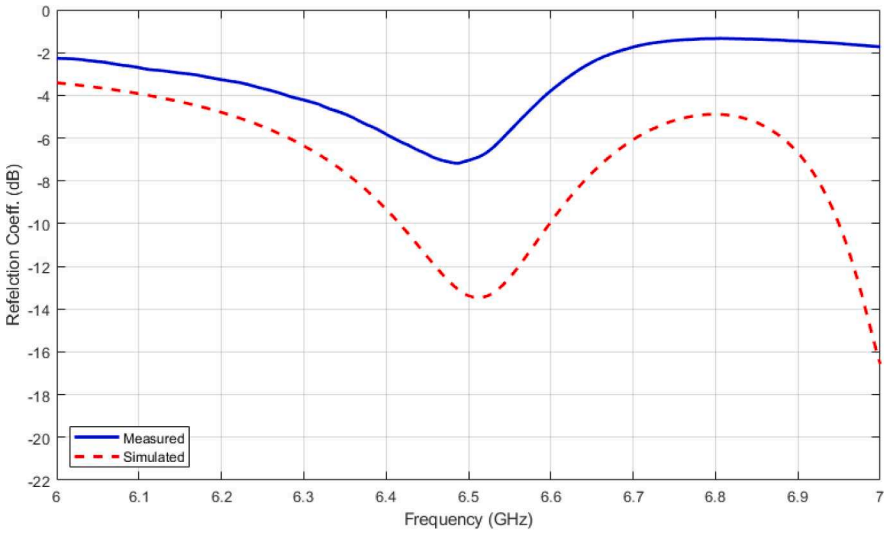

Fig. 8. Simulated and measured reflection coefficient of the 3D printed metamaterial antenna.

achieved minimum reflection coefficient value is typical of miniaturised/wearable antennas [21]. The antenna resonates at 6.5 GHz and has a maximum efficiency of 60.4% at 6.45 GHz, as shown in Fig. 9. The demonstrator is also directional as shown in Fig. 10 due to the addition of the AMC; the measured directivity and gain at 6.5 GHz is 4.64 and 2.34 dBi respectively. For reference, typically a monopole (with dipole-like radiation pattern) exhibit directivity values of approximately 2.15 dBi. To increase the directivity of the demonstrator further, the size of the AMC would also need to be increased as this would redirect the backwards radiation into the forwards direction, however this would naturally increase the overall size, the cost and weight of the antenna. The effect of the AMC can be seen upon the radiation patterns shown in

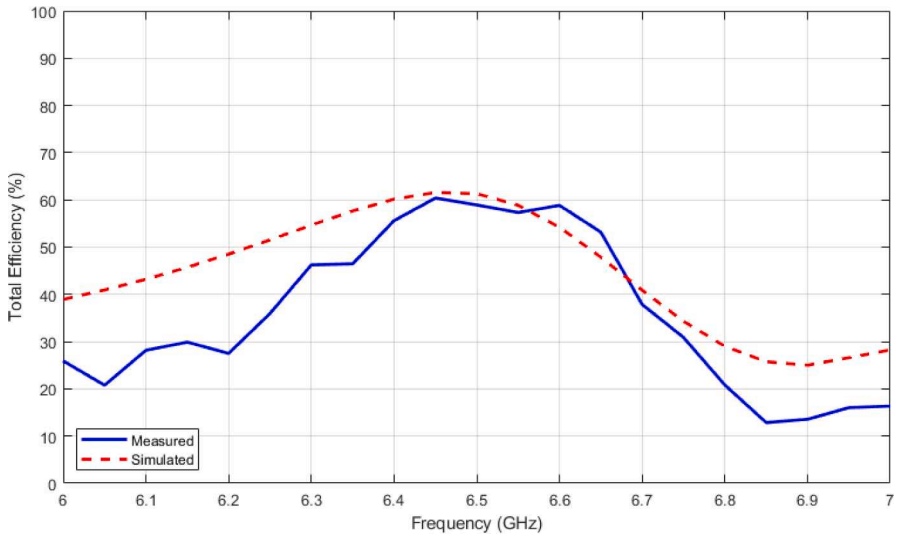

Fig. 9. Measured and simulated efficiency of the metamaterial antenna.

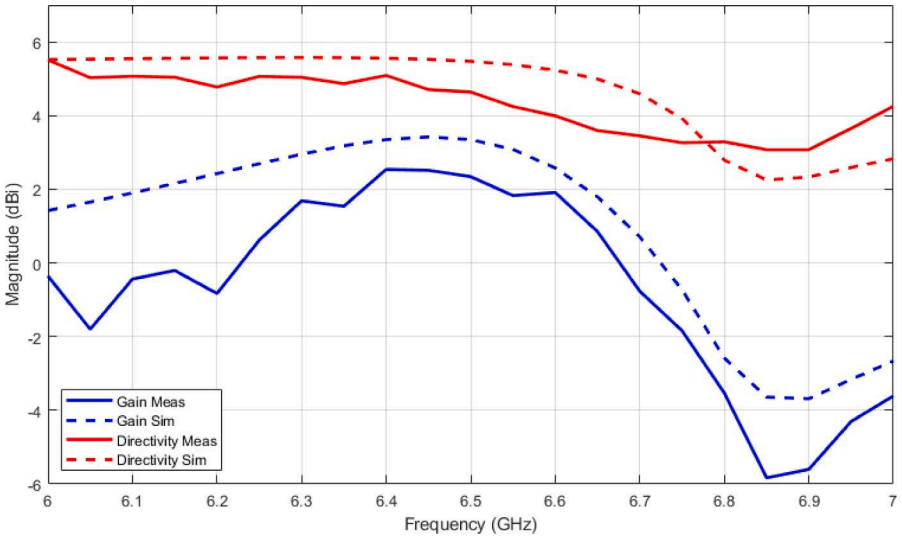

Fig. 10. Measured and simulated directivity and gain of the metamaterial antenna.

Fig. 11, where there is a lower radiation intensity at 180° compared to 0°, and the front to back ratio of the measured antenna was calculated to be 4.58 dB.

4. Conclusions

A multi-material extrusion additive manufacturing process has been used to produce multi-layer three-dimensional test samples using an ultra-low sintering temperature microwave ceramic material, Ag_2MoO_4 (AMO), and silver paste.

AMO green bodies were printed and fired at 480 °C for 1 h, resulting in ceramic bodies of $\rho_{rel} = 88.45 \pm 0.48\%$, $\varepsilon_r = 10.99 \pm 0.04$, $Q \times f = 2597 \pm 540$ GHz and $\tan\delta = 0.005 \pm 0.001$.

Hybrid processing by combining microwave and convention sintering at 480 °C while applying 2 kW microwave energy for a total duration of 60 min, resulted in defect-free metal/ceramic structures using Ag/AMO.

Finally, a metamaterial antenna structure with a metallic artificial magnetic conductor was fabricated, to demonstrate for the first time, the potential of combining multi-material additive manufacturing and microwave-assisted sintering, to produce fully functional metal/ceramic structures.

CRediT authorship contribution statement

Athanasios Goulas: Conceptualization, Methodology, Investigation, Visualization, Writing – original draft. **Tom Whittaker:** Investigation, Methodology, Writing – review & editing. **George Chi-Tangyie:** Investigation, Methodology, Writing – review & editing. **Ian M. Reaney:** Conceptualization, Supervision, Writing – review & editing. **Daniel Engstrøm:** Conceptualization, Supervision, Writing – review & editing. **Will Whittow:** Conceptualization, Supervision, Writing – review & editing. **Bala Vaidhyanathan:** Conceptualization, Supervision, Writing – review & editing.

Declaration of Competing Interest

The authors declare that they have no known competing financial interests or personal relationships that could have appeared to influence the work reported in this paper.

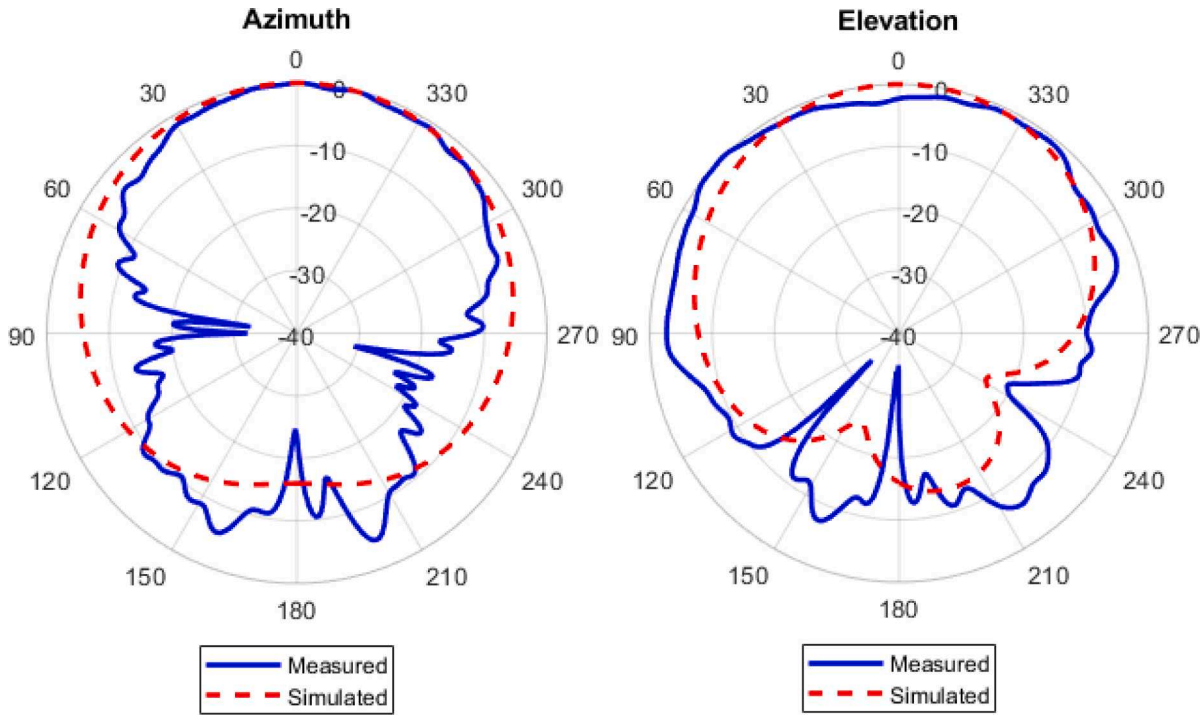

Fig. 11. Measured and simulated far field radiation patterns at 6.45 GHz of the AMC backed monopole, (a) azimuth plane, (b) elevation plane.

Data availability

Data will be made available on request.

Acknowledgments

This work was supported by EPSRC research grant SYMETA (EP/N010493/1). The authors would like to thank the experimental officers in the Loughborough Materials Characterisation Centre (LMCC) for their assistance.

References

[1] J. Varghese, N. Joseph, H. Jantunen, S.K. Behera, H.T. Kim, M.T. Sebastian, Microwave Materials for Defense and Aerospace Applications, in: Handbook of Advanced Ceramics and Composites, Springer International Publishing, 2020, pp. 165–213, https://doi.org/10.1007/978-3-030-16347-1_9.

[2] D. Zhou, L.X. Pang, D.W. Wang, C. Li, B.B. Jin, I.M. Reaney, High permittivity and low loss microwave dielectrics suitable for 5 G resonators and low temperature co-fired ceramic architecture, J. Mater. Chem. C Mater. 5 (2017) 10094–10098, https://doi.org/10.1039/c7tc03623j.

[3] I.M. Reaney, D. Iddles, Microwave dielectric ceramics for resonators and filters in mobile phone networks, J. Am. Ceram. Soc. 89 (2006) 2063–2072, https://doi.org/10.1111/j.1551-2916.2006.01025.X.

[4] D. Zhou, W.B. Li, L.X. Pang, J. Guo, Z.M. Qi, T. Shao, Z.X. Yue, X. Yao, Sintering behavior and dielectric properties of ultra-low temperature fired silver molybdate ceramics, J. Am. Ceram. Soc. 97 (2014) 3597–3601, https://doi.org/10.1111/jace.13159.

[5] R. Gheisari, H. Chamberlain, G. Chi-Tangyie, S. Zhang, A. Goulas, C.K. Lee, T. Whittaker, D. Wang, A. Ketharam, A. Ghosh, B. Vaidhyanathan, W. Whittow, D. Cadman, Y.C. Vardaxoglou, I.M. Reaney, D.S. Engstrøm, Multi-material additive manufacturing of low sintering temperature $Bi_2Mo_2O_9$ ceramics with Ag floating electrodes by selective laser burnout, Virtual Phys. Prototype 15 (2020) 133–147, https://doi.org/10.1080/17452759.2019.1708026.

[6] A. Goulas, G. Chi-Tangyie, D. Wang, S. Zhang, A. Ketharam, B. Vaidhyanathan, I. M. Reaney, D.A. Cadman, W.G. Whittow, J.Y.C. Vardaxoglou, D.S. Engstrøm, Additively manufactured ultra-low sintering temperature, low loss $Ag_2Mo_2O_7$ ceramic substrates, J. Eur. Ceram. Soc. 41 (2020) 394–401, https://doi.org/10.1016/j.jeurceramsoc.2020.08.031.

[7] J. Kim, S.C. Mun, H.U. Ko, K.B. Kim, M.A.H. Khondoker, L. Zhai, Review of microwave assisted manufacturing technologies, Int. J. Precis. Eng. Manuf. 13 (2012) 2263–2272, https://doi.org/10.1007/s12541-012-0301-2.

[8] L. Ćurković, R. Veseli, I. Gabelica, I. Žmak, I. Ropuš, M. Vukšić, A review of microwave-assisted sintering technique, Trans. Famena 45 (2021), https://doi.org/10.21278/TOF.451021220.

[9] C. Leonelli, P. Veronesi, L. Denti, A. Gatto, L. Iuliano, Microwave assisted sintering of green metal parts, J. Mater. Process. Technol. 205 (2008) 489–496, https://doi.org/10.1016/j.jmatprotec.2007.11.263.

[10] R.V. Batienkov, A.N. Bol'shakova, A.A. Khudnev, Microwave sintering of metal powder materials (review), Metallurgist (2021) 82–91, https://doi.org/10.52351/00260827_2021_10_82.

[11] C. Singh, V. Khanna, S. Singh, Sustainability of microwave heating in materials processing technologies, Mater. Today Proc. 73 (2023) 241–248, https://doi.org/10.1016/j.matpr.2022.07.216.

[12] C. Lee, J. McGhee, C. Tsipogiannis, S. Zhang, D. Cadman, A. Goulas, T. Whittaker, R. Gheisari, D. Engstrom, J. Yiannis Vardaxoglou, W. Whittow, Evaluation of microwave characterization methods for additively manufactured materials, Designs 3 (2019), https://doi.org/10.3390/designs3040047.

[13] A. Goulas, S. Zhang, D.A. Cadman, J. Järveläinen, V. Mylläri, W.G. Whittow, J.Y. C. Vardaxoglou, D.S. Engstrøm, The impact of 3D printing process parameters on the dielectric properties of high permittivity composites, Designs 3 (2019), https://doi.org/10.3390/designs3040050.

[14] N. Doebelin, R. Kleeberg, Profex: a graphical user interface for the Rietveld refinement program BGMN, J. Appl. Crystallogr. 48 (2015) 1573–1580, https://doi.org/10.1107/S1600576715014685.

[15] G.Q. Zhang, J. Guo, H. Wang, Ultra-low temperature sintering microwave dielectric ceramics based on Ag_2O–MoO_3 binary system, J. Am. Ceram. Soc. 100 (2017) 2604–2611, https://doi.org/10.1111/jace.14760.

[16] D. Wang, D. Zhou, K. Song, A. Feteira, C.A. Randall, I.M. Reaney, Cold-sintered C0G multilayer ceramic capacitors, Adv. Electron. Mater. 5 (2019) 1–5, https://doi.org/10.1002/aelm.201900025.

[17] D. Wang, S. Zhang, D. Zhou, K. Song, A. Feteira, J.C. Vardaxoglou, W. Whittow, D. Cadman, I.M. Reaney, Temperature stable cold sintered $(Bi_{0.95}Li_{0.05})(V_{0.9}Mo_{0.1})O_4$-$Na_2Mo_2O_7$ microwave dielectric composites, Materials (2019) 12, https://doi.org/10.3390/ma12091370.

[18] J. Perelaer, B.J. De Gans, U.S. Schubert, Ink-jet printing and microwave sintering of conductive silver tracks, Adv. Mater. 18 (2006) 2101–2104, https://doi.org/10.1002/adma.200502422.

[19] M. Figueroa, K. Pourrezaei, S. Tyagi, Microwave monitoring of silver nanoparticle sintering for surface-enhanced Raman scattering substrates, J. Raman Spectrosc. 43 (2012) 588–591, https://doi.org/10.1002/jrs.3073.

[20] S. Głowniak, B. Szczęśniak, J. Choma, M. Jaroniec, Advances in microwave synthesis of nanoporous materials, Adv. Mater. 33 (2021), https://doi.org/10.1002/adma.202103477.

[21] D. Kearney, M. John, M.J. Ammann, Miniature ceramic dual-PIFA antenna to support band group 1 UWB functionality in mobile handset, IEEE Trans. Antennas Propag. 59 (2011) 336–339, https://doi.org/10.1109/TAP.2010.2090485.